Inorganic Chemistry
Article
Cite This: Inorg. Chem. 2018, 57, 9907−9917
pubs.acs.org/IC

Tuning the Redox Potentials and Ligand Field Strength of Fe(II) Polypyridines: The Dual π-Donor and π-Acceptor Character of Bipyridine

Daniel C. Ashley and Elena Jakubikova*

Department of Chemistry, North Carolina State University, Raleigh, North Carolina 27695, United States

Supporting Information

ABSTRACT: The quintet−singlet energy difference ($\Delta E_{Q/S}$) in Fe(II) polypyridine complexes is often interpreted in terms of metal−ligand π interactions. DFT calculations on a series of substituted $[Fe(bpy)_3]^{2+}$ (bpy = 2,2′-bipyridine) complexes show the disparate magnitudes of substituent effects on tuning $\Delta E_{Q/S}$ and reduction potentials ($E°$). In this series, $E°$ spans a much larger range than $\Delta E_{Q/S}$ (2.07 vs 0.29 eV). While small changes in $\Delta E_{Q/S}$ are controlled by metal−ligand π interactions, large changes in $E°$ arise from modification of the electrostatic environment around the Fe center. Molecular orbital analysis reveals that, contrary to the typical description of bpy as a π-acceptor, bpy is better described as acting as both a π-donor and π-acceptor in $[Fe(bpy)_3]^{2+}$ complexes, even when it is substituted with highly electron withdrawing substituents. Overall, substituent modification is a useful strategy for fine-tuning the ligand field strength but not for significant reordering of the spin-state manifold, despite the large effect on metal−ligand electrostatic interactions.

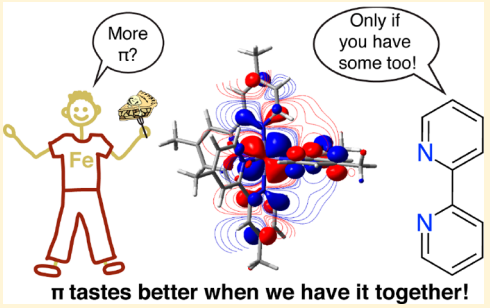

INTRODUCTION

Iron(II) polypyridines have been extensively studied for their numerous applications in the fields of spin crossover (SCO) and photochemistry.[1−3] The ability to precisely control and predict the SCO behavior of transition-metal complexes would have a tremendous effect on multifunctional material design.[4] Knowledge of spin-state energetics is generally useful for understanding excited-state photophysics[5−7] and problems involving two-state reactivity.[8,9] While SCO often involves solid-state effects, at its core it is ultimately a molecular problem[10] and as such is amenable to interpretation through traditional electronic structure theory concepts in tandem with experiment.[11,12] A recent study by Halcrow and Deeth examined a series of substituted $[Fe(bpp)_2]^{2+}$ (bpp = 2,6-di{pyrazol-1-yl}pyridine) complexes and investigated the effect of changing substituents at differing positions on the bpp ring(s).[13] This work concluded that the substituent effects on the quintet−singlet energy gap ($\Delta E_{Q/S}$) were due to modification of both σ- and π-donor properties of the bpp ligand, with substituents at the para position of the pyridyl ring primarily affecting $\Delta E_{Q/S}$ by altering ligand π-back-bonding. The dependence of $\Delta E_{Q/S}$ on ligand donor strength made chemical sense, and it inspired us to explore the related issue of quantifying how sensitive these spin-state energetics are to changes in substituent electron-donating/-withdrawing character.

Ligand substitutions at sterically unhindered positions are sometimes utilized as a strategy to tune the spin-state energetics of first-row transition-metal complexes via electronic effects.[14,15] For example, one would expect that, in a complex where the ligand acts as a π acceptor, substitution of an electron-withdrawing group onto the scaffold will stabilize the energies of ligand π* orbitals. This will bring the π* orbitals closer in energy to the t_{2g} orbitals, increasing interaction between them and, as a result, stabilize the energy of the bonding combination of t_{2g}−π* (HOMO) and increase the Δ_o value (t_{2g}−e_g gap). A change in the redox potential that corresponds to the oxidation of the metal center (i.e., removal of the electron from the HOMO of the transition-metal complex) can then be taken as a measure of this stabilization and the change in the Δ_o value of the complex.[16] Addition of the electron-withdrawing and -donating groups, however, modifies the electrostatic environment of the metal center as well, affecting energies of all molecular orbitals of the complex, which will also be reflected in the change in the metal-centered oxidation potential (see Figure 1). The change in redox potential therefore reflects both effects—the electrostatic effect of stabilization/destabilization of all orbital energies as well as the changes in the HOMO energy due to the changes in the bonding interactions with the ligand. Hence the question we are aiming to answer is as follows: to what extent is the change in the measured redox potential due to changes in the metal−ligand orbital interactions as a function of ligand substitution? In other words, should large changes in substituent electron-donating/-withdrawing character elicit large changes in ligand π-donor/-acceptor strength and $\Delta E_{Q/S}$? Is a change in the

Received: April 12, 2018
Published: August 8, 2018

DOI: 10.1021/acs.inorgchem.8b01002
Inorg. Chem. 2018, 57, 9907−9917

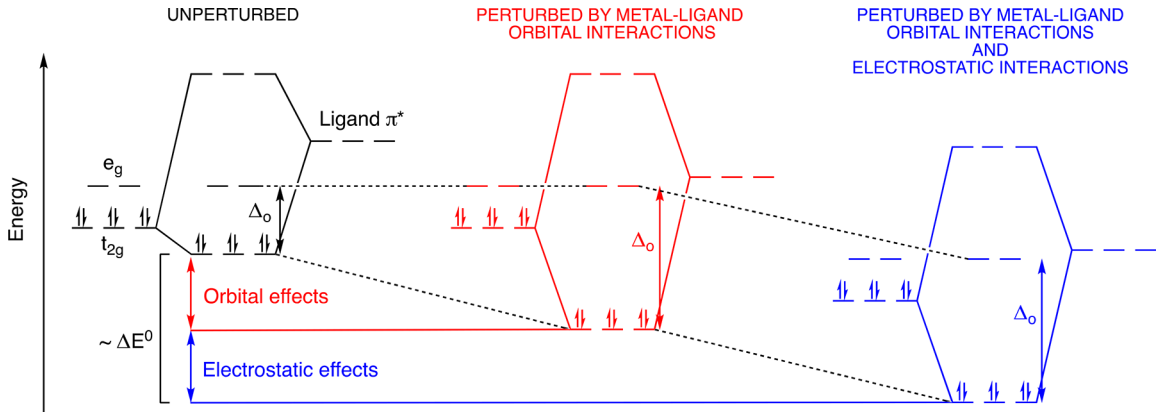

Figure 1. MO interaction diagram illustrating how both metal−ligand orbital and electrostatic interactions lead to the change in $E°$ upon ligand substitution.

redox potential of the metal center a good quantitative measure of the change in $\Delta E_{Q/S}$?

To address this, density functional theory (DFT) calculations were performed on a series of substituted (Y) complexes based on the complex $[Fe(bpy^Y)_3]^{2+}$ (bpy = 2,2′-bipyridine; see Figure 2), with substituents spanning a large

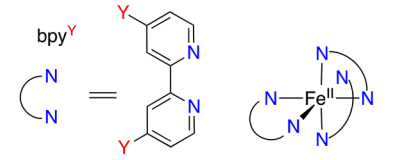

Figure 2. Complexes examined in this study.

range of electron-donating and -withdrawing groups. The goal was to investigate the effect of the ligand modifications on $\Delta E_{Q/S}$, as well as the standard reduction potentials ($E°$) of the Fe(III/II) couple of the series, with more positive reduction potentials corresponding to more electron deficient Fe(II) centers. Interestingly, we found that, while large changes in substituent electron donor strength caused large changes in $E°$, they only had a minor effect on $\Delta E_{Q/S}$ in this system. This is a consequence of substituent effects affecting M−L electrostatics more substantially than orbital interactions, as shown by energy decomposition analysis (EDA). In the course of this investigation fragment molecular orbital analysis (FMOA) showed that classifying bpy as a π acceptor, as is commonly done in the literature and textbooks,[17−25] is potentially misleading. Rather, the bipyridine ligand in Fe(II) complexes has a dual π-acceptor/π-donor character, with neither interaction being small enough to outright ignore.

COMPUTATIONAL METHODOLOGY

All structures were optimized with the BP86[26,27] functional. The 6-311G* basis set was used on all light atoms,[28−32] while the SDD basis sets and accompanying pseudopotentials were used for Fe and I.[33,34] An ultrafine integral grid was employed for all calculations. All calculations incorporated solvation via the IEF-PCM implicit solvation model to simulate the effect of acetonitrile (ε = 37.5). Singlets were run as unrestricted calculations, and stability analysis was always performed to confirm that the closed-shell solution was the lowest in energy. Frequencies were calculated for all optimized structures using the harmonic oscillator approximation to verify that the structures were true minima with no imaginary frequencies. The results of these frequency calculations were also used to calculate zero-point energy and entropic corrections to the free energy at 298.15 K and 1.0 atm using standard statistical mechanical conventions. All DFT calculations were performed with the Gaussian 09 software package (Revision D.01).[35] Mulliken population analysis (MPA), EDA, and FMOA were performed using AOMix 6.90.[36,37] Natural bond orbital (NBO) analysis was also conducted to support the FMOA, and this was performed with NBO 6.0.[38] For analysis of orbital energies it was always very easy to identify three orbitals that were "t_{2g}-like" and their energies were averaged. These three orbitals were not degenerate due to the lower symmetry of the complexes, with the spread in their orbital energies ranging from 0.15 to 0.25 eV. Usually it was simple to identify two orbitals that were "e_g-like" as well, but in some cases the "e_g" character was broken up over several additional orbitals. All orbitals with the "e_g" character and %Fe composition more than ∼10% were included when the energy was averaged.

Note that both EDA and FMOA involved calculations on an isolated Fe(II) ion. As these particular analyses were focused on the singlet state of $[Fe(bpy^Y)_3]^{2+}$ complexes, the Fe(II) ion was calculated as a singlet, rather than a quintet. This was done to avoid having to invoke an irrelevant spin flip when the metal complex was formed in the singlet state. Technically, a spin flip must now be invoked at some point for the binding energy calculations of the quintet case, which is analyzed briefly for the EDA. However, as this only causes a constant shift in the calculated values, issues related to the reference state of the Fe(II) ion are ultimately inconsequential for analysis of the trends in our data, which is the goal of the paper.

Reduction potentials ($E°$) were determined relative to the normal hydrogen electrode (NHE) through eq 1:

$$E° \text{ (eV)} = -\frac{\Delta G_{sol}}{nF} - 4.43 \quad (1)$$

Here, ΔG_{sol} is the change in solvated free energy upon reduction, n is the number of electrons transferred (in our case this is always 1), and F is Faraday's constant. The specific reaction in question is the reduction of the Fe(III) complex (in the doublet state) to the Fe(II) complex (in the singlet state). The calculated potentials are referenced to NHE by subtracting the estimated absolute reduction potential of NHE, 4.43 V.[39] Note that there have been newer estimates of this value and not all of them agree;[40−45] hence, our calculated values may be subject to a modest systematic error. This will have no significant effects on our major conclusions, however, and this general procedure has been shown to work well in previous computational studies.[46] Furthermore, the calculated reduction potentials were shown to have good agreement with experimental results when the data were available for comparison (see Table S1 and discussion below).

$\Delta E_{Q/S}$ was calculated as the electronic energy of the optimized quintet state minus the electronic energy of the optimized singlet

DOI: 10.1021/acs.inorgchem.8b01002
Inorg. Chem. 2018, 57, 9907−9917

state. The more positive the $\Delta E_{Q/S}$ value, the greater the stability of the singlet state. $\Delta E_{Q/S}$ is notoriously difficult to accurately determine computationally with DFT.[10,11,47−52] Jakubikova and co-workers have demonstrated that, for complexes which undergo similar structural changes upon spin-state interconversion, the functional dependence and hence the *relative* values of $\Delta E_{Q/S}$ should be accurate and consistent regardless of functional choice.[53] Unless mentioned otherwise, $\Delta E_{Q/S}$ will always be reported relative to the value for the unsubstituted $[Fe(bpy)_3]^{2+}$. Note that it is expected[54] that BP86 will overstabilize the singlet state, making the "absolute" values of $\Delta E_{Q/S}$ less useful to analyze. For this system we do note a subtle, but important, functional dependence that did significantly affect the relative values of $\Delta E_{Q/S}$. This phenomenon was very complex and beyond the scope of this study and hence will be published separately; however, for functionals with reasonable amounts of Hartree−Fock exchange (less than 25−30%) the general conclusions remained the same. The BP86 functional was chosen on the basis of the previous study by Halcrow and Deeth,[13] in which it was shown to be highly effective at obtaining a similar relative ordering of $\Delta E_{Q/S}$ in comparison with experimental values.

RESULTS AND DISCUSSION

The results of this study are organized as follows. First, the relationship among $\Delta E_{Q/S}$, Fe(III/II) reduction potentials, and substituent donor strength is established. This is followed by a discussion of the qualitative electronic structure of the Fe(II) complexes studied to help us interpret the observed dependence of the $\Delta E_{Q/S}$ on reduction potentials and substituent donor strength in terms of metal−ligand bonding. A more quantitative population analysis and fragment orbital analysis are presented next, to provide a more rigorous interpretation of the metal−ligand bonding arguments from the previous section. The final section details the results from energy decomposition analysis, which are used to describe the relationship between the metal−ligand bonding and $\Delta E_{Q/S}$.

Redox Potentials and Ligand Field Strength. The redox potential, $E°$, is a physically intuitive way to quantify how the electronic and electrostatic environment of the metal center is affected by the substitution of the bpy ligands. The calculated $E°$ can be then compared to experiment when possible. The computational methodology was found to reproduce experimentally measured values of $E°$ with an excellent agreement (see Figure 3 and Table S1). The DFT calculated values of both $E°$ and $\Delta E_{Q/S}$ were then considered as a function of the electron donor strength of the substituent using experimentally known Hammett parameters[55,56] (σ_p, which will simply be referred to as σ throughout), as shown in Figures 3 and 4, respectively. As the donor strength of the substituent increases, the Fe(II) center becomes more electron rich, and as such $E°$ becomes less positive (Figure 4) in a highly linear fashion, as might be expected. A large range of $E°$, spanning 2.07 eV, was determined for the compounds studied here. Therefore, if there is a strong connection between substituent electron donor strength and $\Delta E_{Q/S}$, it should be readily apparent in this system, as the large range of donor strengths should elicit a correspondingly large effect on $\Delta E_{Q/S}$.

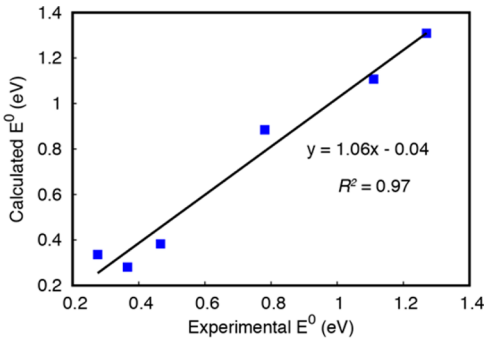

Figure 3. Calculated Fe(III/II) standard reduction potentials vs experimentally determined[23,57] standard reduction potentials shown for all complexes where this comparison was possible. All reduction potentials are reported vs the NHE.

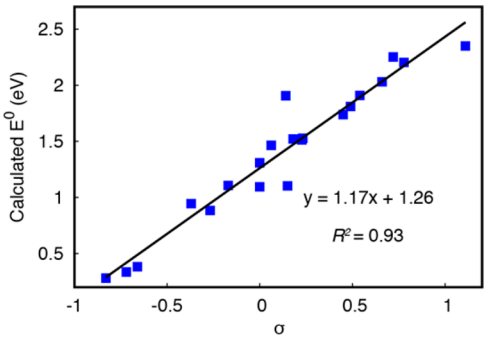

Figure 4. Calculated $E°$ (reported vs NHE) vs σ Hammett parameter of ligand substituents for all complexes considered.

The range of $\Delta E_{Q/S}$ values determined (Figure 5), however, is not particularly large: 0.29 eV (6.69 kcal/mol). Given the massive changes in the $E°$, this is a relatively small "payoff". These results show that modifying the ligand field strength through bpy substitutions, even when they dramatically change the $E°$ value of the metal center, is not necessarily an effective strategy for inducing large changes in the spin-state manifold. The correlation between $\Delta E_{Q/S}$ and σ is rather poor; a better

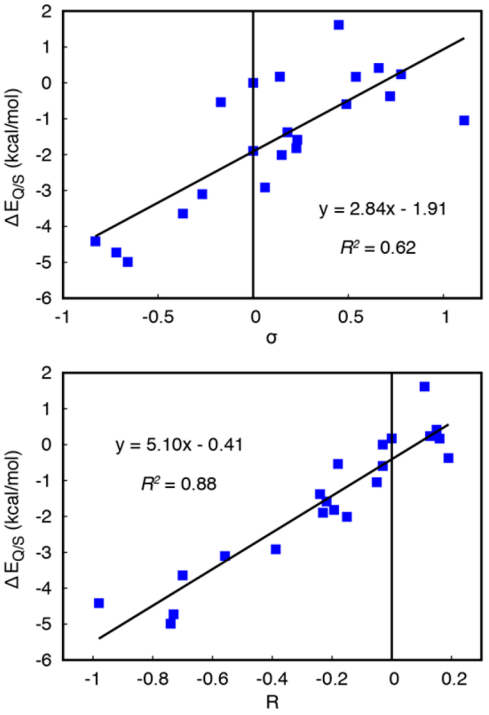

Figure 5. $\Delta E_{Q/S}$ as a function of σ (top) and R (bottom). All values are reported relative to the unsubstituted $[Fe(bpy)_3]^{2+}$ by treating its $\Delta E_{Q/S}$ value as zero.

DOI: 10.1021/acs.inorgchem.8b01002
Inorg. Chem. 2018, 57, 9907−9917

correlation is seen when Hammett parameters that explicitly reflect π interactions are considered. Halcrow and Deeth saw a modest improvement in R^2 on going from σ to σ^+ (0.86 to 0.92),[13] which was seen here as well (0.62 to 0.77). Further improvement is found by using the Swain−Lupton resonance parameter R, which is one way to quantify the contribution of resonance effects to σ.[55,56] Note that R is closely related to Hammett parameters and, like them, is dimensionless. A detailed description of R can be found in ref 55.

Figure 5 shows an increase in the correlation with $\Delta E_{Q/S}$ from $R^2 = 0.62$ ($\Delta E_{Q/S}$ vs σ) to $R^2 = 0.88$ ($\Delta E_{Q/S}$ vs R), which can be taken as evidence that $\Delta E_{Q/S}$ is being largely controlled by changes in the Fe−bpy π-interactions. Note that this does not mean that Fe−bpy π interactions are the ones solely responsible; Halcrow and Deeth suggested that there is a competition between Fe−bpp π interactions and σ interactions, with the dominant interaction being related to the position of the substituent.[13] Additionally, work by Shatruk and co-workers has shown evidence for σ interactions being the dominant factor in dictating spin-state energetics,[17] although their work investigated a broad range of diimine ligands across which σ interactions are expected to vary more widely than in our substituted bpy series. Regardless, given the higher correlation R will generally be used throughout the rest of the paper, but plots of $\Delta E_{Q/S}$ using alternative Hammett parameters are available in Figures S1 and S2 in the Supporting Information.

Electronic Structure of Fe(II) Complexes. To understand the disconnect between the changes in E° and $\Delta E_{Q/S}$, an analysis of the electronic structure of $[Fe(bpy^Y)_3]^{2+}$ was conducted. It was expected that the trends in Figure 5 resulted from an increase in donor strength leading to a decrease in the ability of the bpy^Y ligands to effectively remove electron density from the Fe(II) center through π back-bonding. Such a relationship should be readily visible from analyzing the t_{2g} MOs,[58] which should show π-bonding interactions with the bpy^y ligand. Although symmetry was not strictly enforced in our calculations, the complexes shown in Figure 2 are all formally of D_3 symmetry, which means that the "t_{2g}" orbitals are not actually degenerate; rather, the HOMO is of a_1 symmetry and the HOMO-1 and HOMO-2 are of e symmetry. Because of this, the HOMO-1 and HOMO-2 behave virtually identically in most cases, but differently from the HOMO. The HOMO-1 will be taken as representative of the e pair. For the sake of simplicity, they are still referred to as t_{2g} orbitals belonging to a pseudo-octahedral complex.

Isosurfaces of the calculated t_{2g} MOs of $[Fe(bpy)_3]^{2+}$ do not readily show the aforementioned π-bonding character (Figure 6). Instead, it appears that there is significant π-antibonding character between the metal and the ligands (a feature that can be seen much more clearly in 2D slices also shown in Figure 6). Note that this antibonding interaction is between the metal and the ligands, not necessarily the metal and nitrogen, as there is very little nitrogen character at all, especially in the HOMO-1 (see Figure 7). π-antibonding character itself is consistent with a ligand that acts as a π donor. This is a surprising result in light of the fact that bpy is frequently described as a π-acceptor ligand,[17−25] where this back-bonding is usually considered essential for understanding Fe(II) polypyridine complexes. On the other hand, more in line with the "traditional" view of bpy, there are several low-lying virtual orbitals that are heavily ligand dominated and show π-antibonding interactions as well, which is what would be

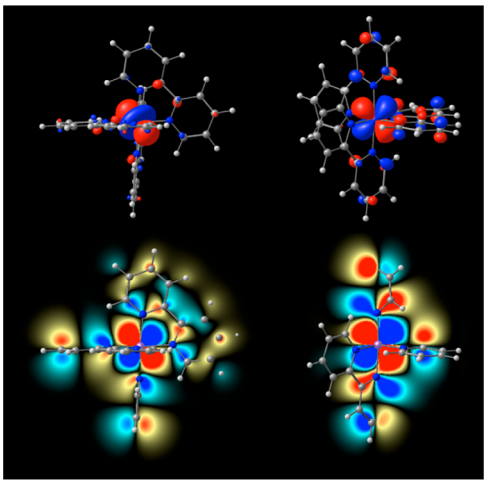

Figure 6. t_{2g} MO isosurfaces (isovalue 0.03 e/Å^3) and 2D slices for the HOMO (left) and HOMO-1 (right) of singlet $[Fe(bpy)_3]^{2+}$. Molecules have been positioned to provide an optimal view of the π character for each orbital.

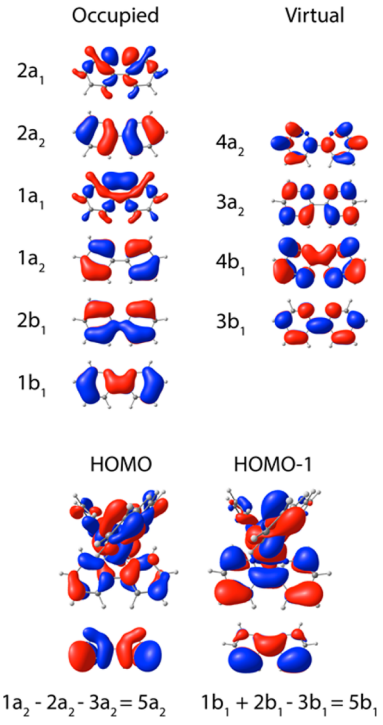

Figure 7. t_{2g} MO isosurfaces for bpy (isovalue 0.03 e/Å^3) and singlet $[Fe(bpy)_3]^{2+}$ (isovalue 0.015 e/Å^3 to make the ligand character more easily visible). The symmetry labels for the bpy orbitals correspond to their irreducible representations in C_{2v} symmetry.

expected for a ligand that acts as a π acceptor. Further adding to the confusion is that the ligand character of the t_{2g} orbitals does not strongly resemble any one of bpy's frontier MOs (Figure 7). This collection of contradictory evidence suggests that bpy is simultaneously acting as a π donor and π acceptor. This possibility was surprising but required deeper analysis to demonstrate its veracity.

If the t_{2g} orbitals result from pure metal orbitals mixing with a combination of filled and unfilled π orbitals due to π-donor/-acceptor interactions, it should be possible to approximate these orbitals from appropriate linear combinations of isolated

DOI: 10.1021/acs.inorgchem.8b01002
Inorg. Chem. 2018, 57, 9907−9917

bpy orbitals (Figure 7). The bpy LUMO is of b_1 symmetry (in C_{2v}), and subtracting it from the sum of the two highest energy filled π-bonding orbitals of b_1 symmetry results in an orbital (labeled as $5b_1$) that looks similar to the ligand character in the HOMO-1. The ligand character in the HOMO is different, as the HOMO itself is of different symmetry from the HOMO-1 and HOMO-2 in D_3. A different combination of a_2 orbitals can be generated to make $5a_2$, which looks similar to the HOMO. Note that these orbitals are not "perfect matches" because they are highly oversimplified (all orbitals contribute equally, no other orbitals contribute, etc.). In general, the complicated ligand character of the t_{2g} orbitals is consistent with both π-donor and π-acceptor interactions with bpy.

Population Analysis. The visual analysis above is highly qualitative, and hence a more quantitative analysis was performed. The trends in $\Delta E_{Q/S}$ are consistent with stronger electron donors decreasing π back-bonding, or increasing π bonding, and these data by themselves cannot resolve which is a better description of the actual bonding behavior. A Mulliken population analysis (MPA) of the t_{2g} MO compositions across the entire series was conducted to further probe the character of this interaction (Figure 8). It was seen that as the donor strength decreases (R becomes more positive) the t_{2g} MOs become increasingly metal dominated, eventually leveling off at the larger R values.

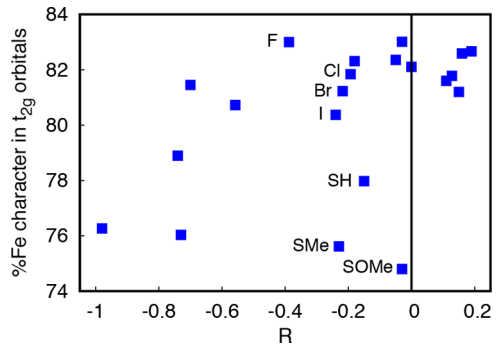

Figure 8. Percentage of Fe character in the t_{2g} KS-MOs for all studied complexes. The percentages of all three "t_{2g}" orbitals were averaged to produce each point on the plot.

Such changes are only consistent with bpy primarily acting as a π donor: making the ligand a weaker donor serves to lessen the Fe–bpy interactions and therefore increases the metal character of the t_{2g} orbitals. The exact opposite effect would be expected if bpy were primarily a π acceptor. Figure 9 illustrates these two trends for simplistic depictions of bpy acting as a pure π acceptor or a pure π donor. Our results suggest, however, that bpy has dual π-donor/π-acceptor character.

There are several clear outliers from this trend in Figure 8: namely, the compounds with Y groups that have lone pairs on sulfur capable of π donation into the bpy ring. The larger halogens can be seen to slightly deviate from the trend as well. Deviations are likely the result of these Y groups being inductively withdrawing (or at least not largely inductively donating) in addition to being able to π-donate through resonance. The data in Figure 8 are averaged for all three t_{2g} orbitals, as they all behave very similarly, with the exception being that for the HOMO orbitals Y = SOMe is much less of an outlier.

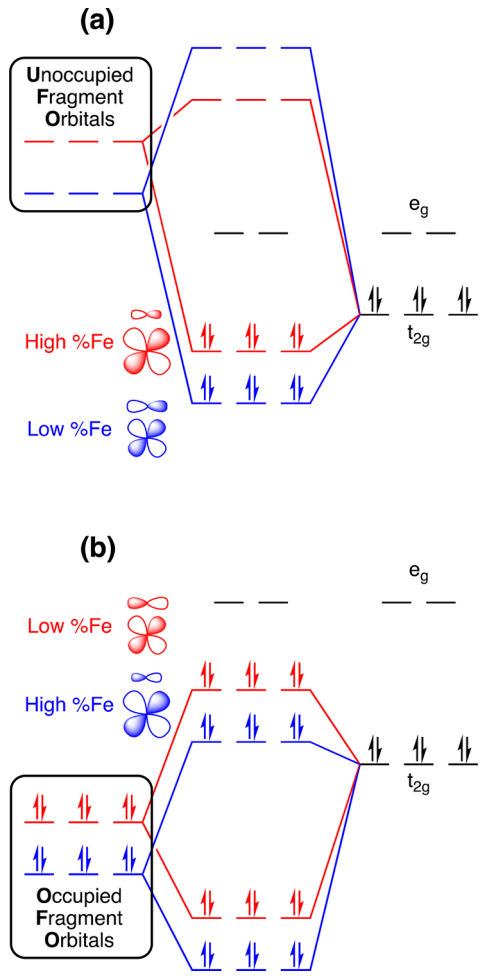

Figure 9. Predicted changes in %Fe composition of t_{2g} MOs and relative MO energies as a function of donor strength for a (a) purely π acceptor ligand and (b) purely π donor ligand. The largest donor strength is shown in red, while the smallest donor strength is shown in blue. Note that, for the π-donor ligand, increasing the donor strength would predict smaller %Fe character in the t_{2g} orbitals, and the opposite is predicted for the π-acceptor ligand.

Fragment Molecular Orbital Analysis (FMOA). A fragment molecular orbital analysis (FMOA)[59] was conducted to more directly demonstrate the π-donor capabilities of bpy in these complexes. The $[Fe(bpy^Y)_3]^{2+}$ molecules were each divided into two fragments, as shown in Figure 10: the Fe(II) ion itself and the supermolecule comprised of all three bpy ligands, referred to as $(bpy^Y)_3$. The composition of the t_{2g} MOs was again examined, but now in terms of what types of fragment orbitals from $(bpy^Y)_3$ were contributing to the final MOs. The ligand fragment orbitals can either be filled or unfilled, and it is this distinction which provides insight into the nature of the metal–ligand interaction. Occupied fragment orbitals (OFOs) chiefly contribute to ligand donation to the metal, while unoccupied fragment orbitals (UFOs) are related to electron acceptance by the ligand from the metal. These fragment orbitals are also indicated in Figure 9.

The OFO and UFO compositions are plotted as a function of R in Figure 11 for the HOMO and the HOMO-1. There is a large decrease in OFO character for both orbitals as R becomes more positive and a simultaneous modest increase in UFO character, consistent with what is expected for less electron rich ligands. For all cases, even for the complexes with the

DOI: 10.1021/acs.inorgchem.8b01002
Inorg. Chem. 2018, 57, 9907–9917

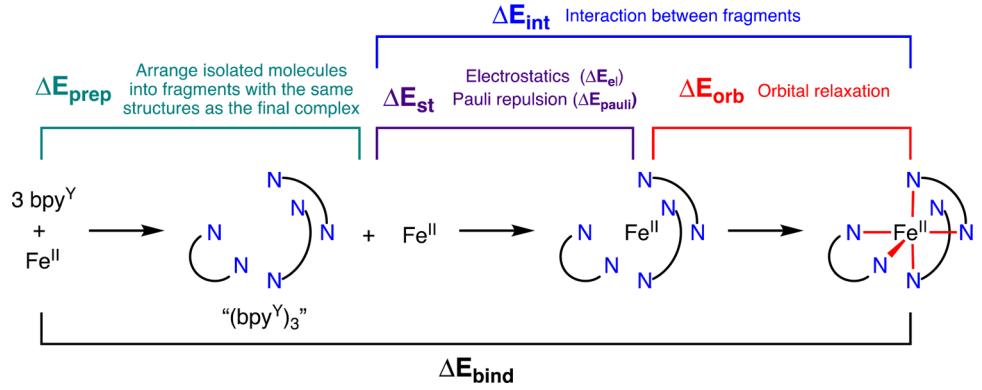

Figure 10. Stepwise scheme of EDA procedure and the fragmentation used for both FMOA and EDA.

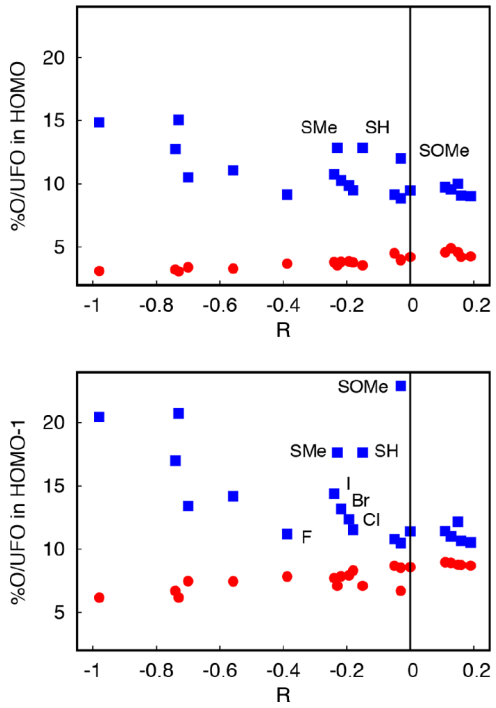

Figure 11. Contribution of OFOs (blue squares) and UFOs (red circles) of the $(bpy^Y)_3$ fragment to the HOMO (top) and HOMO-1 (bottom).

highly electron withdrawing bpy^Y ligands, the ligand has π-donor character comparable to the π-acceptor character, as indicated by the plotted OFO and UFO values (see Figure 11). In fact, the π-donor character is significantly larger than the π-acceptor character in many cases, especially for the HOMO. Therefore, bpy technically acts more like a π donor throughout the entire series. The more important interpretation, however, is that it is not appropriate to discount the dual π-donor/π-acceptor character of bpy. In fact, a similar result has been seen in the composition of the t_{2g} orbitals of $[Ru(bpy)_3]^{2+}$ as well.[24,60] In the present study the combined π-donor/π-acceptor character of bpy is especially evident for the HOMO-1 with highly electron withdrawing ligands, where the OFO and UFO compositions are essentially the same. Note that all of these results are entirely consistent with the qualitative analysis provided earlier, in that the shapes of the t_{2g} MOs are the consequence of both donor and acceptor interactions. The same outliers seen in Figure 8 are present in Figure 11 as well. To investigate whether the results from Figure 11 were an artifact of the MPA, a comparable analysis was performed using NBOs (details in Figure S3 in the Supporting Information and accompanying discussion), and very similar conclusions were reached. One more interesting point is that, for the more electron withdrawing ligands, the HOMO-1 has almost equal π-donor/π-acceptor character. The HOMO however does not and keeps a much larger ratio of π-donor to π-acceptor behavior.

The FMOA also gave another way to quantify π-donor/π-acceptor behavior by providing overlap populations (OPs) between the previously defined fragments in the t_{2g} orbitals (see Figure 10). A positive OP indicates a bonding interaction between two fragments, while a negative value indicates an antibonding interaction. The net OPs for every t_{2g} orbital examined in this study are always negative, demonstrating net antibonding interactions between the Fe(II) ion and the $(bpy^Y)_3$ fragment, as previously seen in the 2-D slices in Figure 6. Further decomposition of these net OPs reveals that they are mainly composed of positive OPs arising from interactions with ligand UFOs (π back-bonding) and negative OPs arising from interactions with ligand OFOs (π donation). The net OPs in the HOMO have a relationship to the substituent donor strength (Figure 12), with the net OPs becoming more

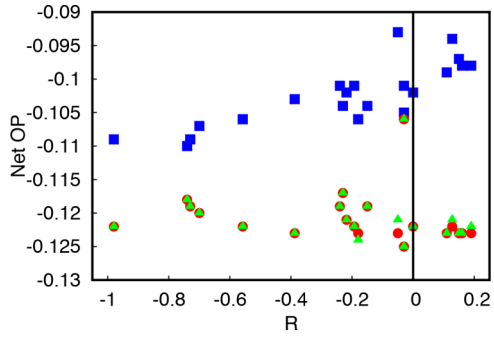

Figure 12. Net OPs calculated for the HOMO (blue squares), HOMO-1 (red circles), and HOMO-2 (green triangles).

positive as the substituent becomes more electron withdrawing: consistent with less π donation and/or more π acceptance. The correlation is not strong, $R^2 = 0.68$, but it is much larger than it is for the HOMO-1 and HOMO-2, which have R^2 values close to 0. While one point appears to be a large outlier for HOMO-1 and HOMO-2 (corresponding to Y = SOMe, the largest outlier in the previous data sets), removal of this point offers little improvement in the correlation. It is

DOI: 10.1021/acs.inorgchem.8b01002
Inorg. Chem. 2018, 57, 9907−9917

possible that the HOMO alone shows a trend because it maintains a higher π-donor/π-acceptor character for the more electron withdrawing substituents, as seen in Figure 11.

Energy Decomposition Analysis (EDA). Having clarified the nature of the covalent interactions between the bpy ligands and Fe(II), the task still remains to determine why the trends in $\Delta E_{Q/S}$ are so small in comparison to the trends in E°. This can be understood by recognizing that the substituents have very different effects on the electrostatic component of Fe−ligand bonding in comparison to the covalent component, which is demonstrated here using EDA.

Figure 10 shows how Ziegler−Rauk/Morokuma[61,62] EDA may be used to analyze the simultaneous binding energy of all three bpy ligands to Fe (ΔE_{bind}). ΔE_{bind} is the sum of the preparation energy (ΔE_{prep}) and the interaction energy (ΔE_{int}). ΔE_{prep} is the energy required to distort the isolated fragments into their final geometries in the optimized complex. As the Fe^{2+} ion cannot structurally change, ΔE_{prep} is only related to the energy involved in arranging the three isolated bpy ligands into the geometry of the $(bpy^{Y})_3$ fragment. ΔE_{prep} will always be positive and unfavorable for any system. In this case it is primarily because it involves pointing the lone pairs of all three bpy ligands toward each other without the Fe^{2+} ion to mitigate unfavorable electrostatic repulsions. The definition of ΔE_{prep} also includes the energetic penalty of distorting the bpy ligands from their natural geometries as isolated molecules, but this effect will be less significant in this case in comparison to the energy involved in bringing the distorted ligands together.[63]

The energy released upon the two static fragments, $(bpy^{Y})_3$ and Fe^{2+}, coming together to form the actual metal complex is referred to as the interaction energy (ΔE_{int}). ΔE_{int} is divided into three additional terms, ΔE_{el}, ΔE_{Pauli}, and ΔE_{orb} (see Figure 10). ΔE_{el} and ΔE_{Pauli} reflect the electrostatic and Pauli repulsion interactions, respectively, and arise from bringing the two fragments together, but without allowing the electronic structure of the molecule to relax (i.e., no orbital optimization). The interaction of the nitrogen lone pairs with the Fe^{2+} center will always be favorable from an electrostatic standpoint (negative ΔE_{el}) but will be compensated to some extent by the Pauli repulsion necessary to bring any two electron-containing fragments together (positive ΔE_{Pauli}). The sum of these two terms is sometimes referred to as ΔE_{st} for "steric" interactions, as will be done here.[64] ΔE_{orb} accounts for the energy released (it will always be negative) by allowing the orbitals to interact with each other and form the final optimized KS-wave function.

The calculated ΔE_{int} values are plotted alongside ΔE_{orb} in Figure 13 as a function of R. As R becomes more negative (donor strength increases), ΔE_{int} becomes significantly more favorable, spanning approximately 80 kcal/mol. ΔE_{int} is the sum of ΔE_{st} and ΔE_{orb}, but the plot of ΔE_{orb} shows a completely different trend where ΔE_{orb} becomes less favorable as R becomes more negative. This is consistent with more electron deficient ligands minimizing the repulsive filled−filled interaction associated with π donation and/or maximizing the stabilizing interaction associated with π acceptance. In addition to showing an entirely different trend, the magnitude of the changes in ΔE_{orb} is much smaller (compare the slopes of the lines), spanning approximately 15 kcal/mol. Necessarily this means that the trend in ΔE_{int} is largely dictated by ΔE_{st}. While we have not separated the electrostatic effect from the Pauli repulsion in this study, it is likely that changes in ΔE_{el} are more important than changes in ΔE_{Pauli}. An increase in donor strength should lead to more favorable electrostatic interactions but also more unfavorable Pauli repulsion. As ΔE_{st} becomes substantially more favorable with increasing donor strength, it is clear that the increased electrostatic attraction more than compensates for the increased Pauli repulsion between the two fragments. It will then be assumed from here on that the most important term for interpreting ΔE_{st} is ΔE_{el} and that the changes in ΔE_{Pauli} are not relevant for the questions at hand.

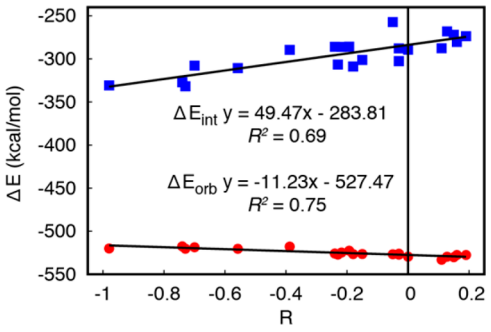

Figure 13. ΔE_{int} (blue squares) and ΔE_{orb} (red circles) plotted as a function of R.

Electrostatic effects and covalent effects all contribute significantly to the Fe−ligand interactions. However, substituent effects only cause small changes in the covalent component and much larger changes in the electrostatic component of the interaction energy. The ligand substituent effects have large consequences for the electrostatic nature of bonding, and hence the electrostatic environment of the Fe(II) center, which results in the large range of reduction potentials. The covalent substituent effects are less dramatic and are connected to the π interactions responsible for tuning the spin-state energies, resulting in a smaller range for $\Delta E_{Q/S}$.

From an MO standpoint, the electrostatic effects of ligand substitution shift the energies of the t_{2g} and e_g* MOs significantly but by similar amounts (see Figure 14), which results in large changes in the electron affinity of the complexes, but not the actual ligand field splitting itself. A similar shifting of MO energies was shown in Halcrow and Deeth's work, where they focused on the slopes of the lines to indicate whether π or σ donation was dominant, and we saw good agreement with their results.[13] Just as in their study, the slope of the t_{2g} energies is slightly more negative than it is for the e_g* energies, showing that the t_{2g} orbitals are more affected by changes in donor strength. It is possible to interpret these changing orbital energies as being largely unrelated to electrostatic effects and instead assume that they are the result of less electron donating ligands exhibiting weaker π donation and/or stronger π back-bonding and weaker σ donation, which together would produce the same qualitative effect. If the effects are similar in magnitude, then they can also partially cancel each other out, resulting in the small changes observed for ΔE_{orb}.

While such compensating effects are no doubt present, it is highly unlikely these are responsible for the large changes in MO energies and reduction potentials. It makes sense that a significant electrostatic shift should be present, given the massive effect ligand substitution has on ΔE_{st}. One way to confidently demonstrate this electrostatic effect, and separate it from orbital-covalency effects, is to analyze the energies of

DOI: 10.1021/acs.inorgchem.8b01002
Inorg. Chem. 2018, 57, 9907−9917

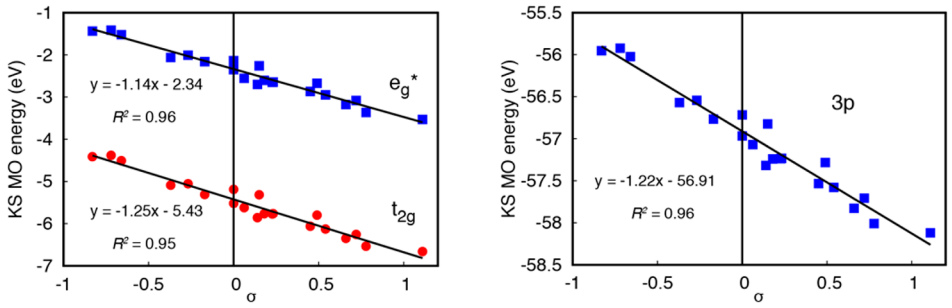

Figure 14. Calculated MO energies as a function of σ. Energies of each set were averaged to produce the values on the plot.

metal-based orbitals that are unambiguously nonbonding. Nonbonding orbitals such as these should still be influenced by the electrostatics but will not undergo any covalent interactions with the ligand. Figure 14 shows the effect of donor strength on the low-lying, nonbonding Fe 3p orbitals, which is remarkably similar to what is seen for the t_{2g} and e_g* orbitals. In fact, no matter which orbital set is considered, they all vary by ~2.2 V across the entire series, a magnitude which excellently predicts the range of reduction potentials calculated. In terms of $\Delta E_{Q/S}$, however, it is interesting to note that the calculated e_g*-t_{2g} gap covers a span of 5.3 kcal/mol, similar to the 6.6 kcal/mol range of $\Delta E_{Q/S}$ calculated, and the two parameters actually correlate quite well (R^2 = 0.92; see Figure S4).

The different trends in ΔE_{int} and ΔE_{orb} (see Figure 13) offer simple explanations for why changes in substituent donor strength can have a large effect on redox potentials and interaction energies but only a small effect on $\Delta E_{Q/S}$. Another explanation is available, however, by focusing on the so far neglected component of ΔE_{bind}, which is ΔE_{prep}. Because the binding energy for the singlet and quintet (see eqs 2 and 3) are both calculated using the same fragments, it is possible to express $\Delta E_{Q/S}$ in terms of the difference in binding energies for each spin state, referred to as $\Delta\Delta E_{bind}(Q/S)$ (eq 4). As before, $\Delta\Delta E_{bind}(Q/S)$ itself can be separated into $\Delta\Delta E_{prep}(Q/S)$ and $\Delta\Delta E_{int}(Q/S)$, which are the differences in preparation and interaction energies for the quintet and singlet, respectively:

$$\Delta E_{bind}(S) = \Delta E_{prep}(S) + \Delta E_{int}(S) \quad (2)$$

$$\Delta E_{bind}(Q) = \Delta E_{prep}(Q) + \Delta E_{int}(Q) \quad (3)$$

$$\Delta E_{Q/S} = \Delta E_{bind}(Q) - \Delta E_{bind}(S) = \Delta\Delta E_{bind}(Q/S) = \Delta\Delta E_{prep}(Q/S) + \Delta\Delta E_{int}(Q/S) \quad (4)$$

$\Delta\Delta E_{prep}(Q/S)$ and $\Delta\Delta E_{int}(Q/S)$ do not consider the isolated bpy ligands, as they are the same for each spin state. $\Delta\Delta E_{prep}(Q/S)$ will only reflect how the structure of $(bpy^Y)_3$ changes during the spin-state change. $\Delta\Delta E_{int}(Q/S)$ can then be simply determined as the difference between $\Delta E_{Q/S}$ and $\Delta\Delta E_{prep}(Q/S)$ or from an explicit calculation of ΔE_{int} for each spin state.

Figure 15 shows how $\Delta\Delta E_{prep}(Q/S)$ changes as a function of substituent donor strength. As the ligand becomes more electron rich, $\Delta\Delta E_{prep}(Q/S)$ becomes less positive. Note that this is the same general trend (and spans a similar range) as that observed for $\Delta E_{Q/S}$, suggesting that $\Delta\Delta E_{prep}(Q/S)$ may be useful for predicting trends in spin-state energetics. The trend in Figure 15 is easy to understand: in all cases $\Delta\Delta E_{prep}(Q/S)$ is a negative quantity, signifying that the

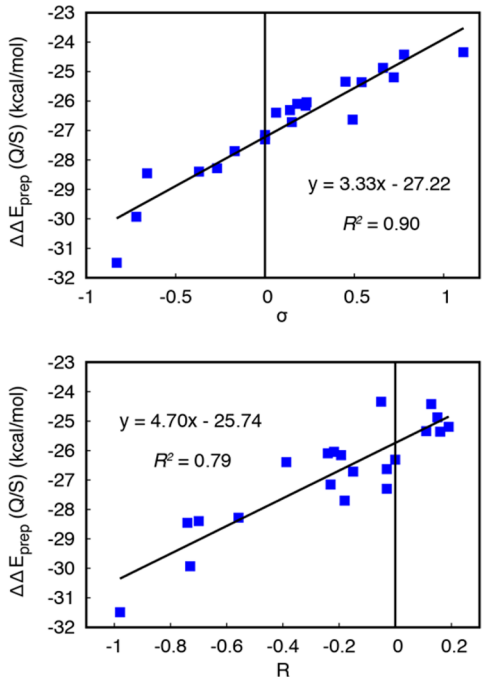

Figure 15. $\Delta\Delta E_{prep}(Q/S)$ as a function of σ (top) and R (bottom).

preparation energy of the quintet state is less unfavorable than the preparation energy of the singlet state. The population of antibonding e_g* orbitals in the quintet state results in longer Fe–N bonds, and therefore larger interligand distances. The electrostatic and filled–filled repulsion energies resulting from the nitrogen lone pairs interacting with each other will be diminished as the interligand distance increases, and this effect will be magnified for the more electron rich ligands. It has been shown previously that repulsive interligand effects (as gauged through calculated preparation energies) can have significant effects on spin-state energetics, often resulting in unexpected ground spin states.[65]

Analysis of $\Delta\Delta E_{int}(Q/S)$ showed no significant trend across the data series (R^2 = 0.04 and 0.01 when it is plotted against σ and R, respectively; see Figure S5), which indicates that the preparation energies are all that is needed to accurately describe the spin-state energetics. Arguably, $\Delta\Delta E_{int}(Q/S)$ itself is composed of $\Delta\Delta E_{orb}(Q/S)$ and $\Delta\Delta E_{st}(Q/S)$, which may simply have opposing trends. However, calculated trends for these values also show essentially no correlation (Figures S6 and S7). This stems from the fact that, unlike $\Delta E_{orb}(S)$, $\Delta E_{orb}(Q)$ does not show any interpretable trend with donor strength (Figure S8), resulting in no correlation for $\Delta\Delta E_{orb}(Q/S)$. It may be that the trends in $\Delta E_{orb}(Q)$ are

DOI: 10.1021/acs.inorgchem.8b01002
Inorg. Chem. 2018, 57, 9907–9917

simply too subtle to effectively detect above DFT error due to much weaker bonding in the quintet state; at present, however, it is not possible to strongly distinguish this from the possibility that there simply is no relationship with donor strength for $\Delta E_{orb}(Q)$ which would consequently mask any relationships with $\Delta\Delta E_{orb}(Q/S)$. Due to this, we ignored further analysis of "interaction" terms with the quintet state and instead focused on the very clear trend in $\Delta\Delta E_{prep}(Q/S)$.

As both $\Delta\Delta E_{prep}(Q/S)$ and ΔE_{orb} are capable of explaining the trend in $\Delta E_{Q/S}$, it is interesting to evaluate which is the better predictor of $\Delta E_{Q/S}$. Both ΔE_{orb} and $\Delta E_{Q/S}$ correlate better with R than with σ, likely due to R's better representation of resonance effects. On the other hand, $\Delta\Delta E_{prep}(Q/S)$ shows the opposite behavior, where it strongly correlates with σ, and actually the correlation slightly decreases when it is plotted against R (see Figure 15). This is further demonstrated by comparing the correlation of $\Delta\Delta E_{prep}(Q/S)$ and ΔE_{orb} with $\Delta E_{Q/S}$ itself (Figure 16). The correlation is

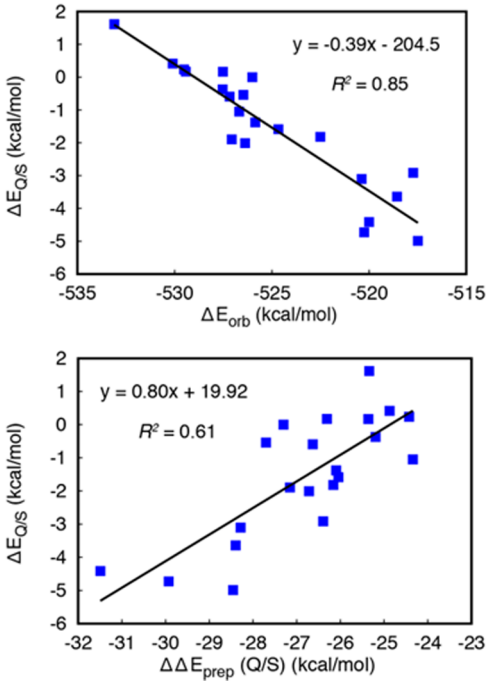

Figure 16. $\Delta E_{Q/S}$ as a function of ΔE_{orb} (top) and $\Delta\Delta E_{prep}(Q/S)$ (bottom).

much worse for $\Delta\Delta E_{prep}(Q/S)$ than for ΔE_{orb}, showing that the latter is a better predictor of the subtle spin-state energetics for this system. On the basis of these results, it is likely that it is a combination of π-orbital effects and interligand interactions that control the observed trends for $\Delta E_{Q/S}$. Regardless of which is more important, $\Delta\Delta E_{prep}(Q/S)$ or ΔE_{orb}, on the basis of the magnitude of these effects it is unlikely that either of these play a dominant role in dictating the trends in reduction potential or Fe−N bond strength, as these are largely governed by the electrostatic effects manifested in ΔE_{st}.

CONCLUSIONS

In this work, we investigate the substituent effects on the redox potential and ligand field strength in a series of $[Fe(bpy^{Y})_3]^{2+}$ complexes (Y = electron-donor and -acceptor groups). Our results show that, even if two Fe(II) complexes have large differences in Fe−ligand bond strength or redox potential, this may not track with a large difference in properties resulting from more covalent interactions, such as $\Delta E_{Q/S}$. Substituent modifications of the bpy scaffold are not an effective way to induce dramatic changes in spin-state energetics, as their effect on covalent interactions as well as interligand interactions is relatively small. However, this means they may be useful for smaller, precise tuning of $T_{1/2}$ values when only a minor adjustment is desired.

A surprising result of this study is that, for $[Fe(bpy^{Y})_3]^{2+}$, bpy shows dual π-donor/π-acceptor character, with the former being similar to or larger than the latter. This result sharply contrasts with the typical description of bpy as a π acceptor. It is not yet clear how general these results are and how much they will change for different ligand types or metals. Current studies are underway in our laboratory to address this. Going forward, it will also be important to carefully investigate the effect of the selected model chemistry (i.e., functional, basis set) as well as the molecular orbital decomposition scheme on the observed π-donor/π-acceptor character of the ligand. Therefore, these results should be taken with due caution until they can be experimentally verified in some way. The conclusions suggested from this study will hopefully serve as an impetus for other experimentalists and theorists to look more closely at these electronic structure issues.

ASSOCIATED CONTENT

Supporting Information

The Supporting Information is available free of charge on the ACS Publications website at DOI: 10.1021/acs.inorgchem.8b01002.

Calculated and experimental Fe(III/II) reduction potentials, calculated $\Delta E_{Q/S}$ values, all Hammett/Swain−Lupton parameters used, alternative NBO-based analysis to corroborate the FMOA presented in the text, various calculated parameters discussed in the text correlated with alternative Hammett/Swain−Lupton parameters, plot of $\Delta E_{Q/S}$ vs e_g−t_{2g} gap, and raw calculated energies for all species considered (PDF)

Cartesian coordinates of all optimized structures (XYZ)

AUTHOR INFORMATION

Corresponding Author

*E-mail for E.J.: ejakubi@ncsu.edu.

ORCID

Daniel C. Ashley: 0000-0002-8838-4269

Elena Jakubikova: 0000-0001-7124-8300

Notes

The authors declare no competing financial interest.

ACKNOWLEDGMENTS

This work was supported by the National Science Foundation (grant CH-1554855). Additionally, we acknowledge the use of the computing resources of the High-Performance Computing Center at NCSU.

REFERENCES

(1) Bousseksou, A.; Molnár, G.; Matouzenko, G. Switching of Molecular Spin States in Inorganic Complexes by Temperature, Pressure, Magnetic Field and Light: Towards Molecular Devices. *Eur. J. Inorg. Chem.* **2004**, *2004*, 4353−4369.

DOI: 10.1021/acs.inorgchem.8b01002
Inorg. Chem. 2018, 57, 9907−9917

(2) Sato, O.; Tao, J.; Zhang, Y. Z. Control of Magnetic Properties through External Stimuli. *Angew. Chem., Int. Ed.* **2007**, *46*, 2152−2187.
(3) Gamez, P.; Costa, J. S.; Quesada, M.; Aromi, G. Iron Spin-Crossover Compounds: From Fundamental Studies to Practical Applications. *Dalton Trans.* **2009**, 7845−7853.
(4) Gaspar, A. B.; Ksenofontov, V.; Seredyuk, M.; Gütlich, P. Multifunctionality in Spin Crossover Materials. *Coord. Chem. Rev.* **2005**, *249*, 2661−2676.
(5) Juban, E. A.; Smeigh, A. L.; Monat, J. E.; McCusker, J. K. Ultrafast Dynamics of Ligand-Field Excited States. *Coord. Chem. Rev.* **2006**, *250*, 1783−1791.
(6) Huse, N.; Cho, H.; Hong, K.; Jamula, L.; de Groot, F. M. F.; Kim, T. K.; McCusker, J. K.; Schoenlein, R. W. Femtosecond Soft X-Ray Spectroscopy of Solvated Transition-Metal Complexes: Deciphering the Interplay of Electronic and Structural Dynamics. *J. Phys. Chem. Lett.* **2011**, *2*, 880−884.
(7) Zhang, W.; Alonso-Mori, R.; Bergmann, U.; Bressler, C.; Chollet, M.; Galler, A.; Gawelda, W.; Hadt, R. G.; Hartsock, R. W.; Kroll, T.; Kjaer, K. S.; Kubicek, K.; Lemke, H. T.; Liang, H. W.; Meyer, D. A.; Nielsen, M. M.; Purser, C.; Robinson, J. S.; Solomon, E. I.; Sun, Z.; Sokaras, D.; Driel, T. B., van; Vanko, G.; Weng, T. C.; Zhu, D.; Gaffney, K. J. Tracking Excited-State Charge and Spin Dynamics in Iron Coordination Complexes. *Nature* **2014**, *509*, 345−348.
(8) Harvey, J. Understanding the Reactivity of Transition Metal Complexes Involving Multiple Spin States. *Coord. Chem. Rev.* **2003**, *238*−*239*, 347−361.
(9) Schröder, D.; Shaik, S.; Schwarz, H. Two-State Reactivity as a New Concept in Organometallic Chemistry. *Acc. Chem. Res.* **2000**, *33*, 139−145.
(10) Paulsen, H.; Schünemann, V.; Wolny, J. A. Progress in Electronic Structure Calculations on Spin-Crossover Complexes. *Eur. J. Inorg. Chem.* **2013**, *2013*, 628−641.
(11) Ashley, D. C.; Jakubikova, E. Ironing out the Photochemical and Spin-Crossover Behavior of Fe(II) Coordination Compounds with Computational Chemistry. *Coord. Chem. Rev.* **2017**, *337*, 97−111.
(12) Rodriguez-Jimenez, S.; Yang, M.; Stewart, I.; Garden, A. L.; Brooker, S. A Simple Method of Predicting Spin State in Solution. *J. Am. Chem. Soc.* **2017**, *139*, 18392−18396.
(13) Kershaw Cook, L. J.; Kulmaczewski, R.; Mohammed, R.; Dudley, S.; Barrett, S. A.; Little, M. A.; Deeth, R. J.; Halcrow, M. A. A Unified Treatment of the Relationship between Ligand Substituents and Spin State in a Family of Iron(II) Complexes. *Angew. Chem., Int. Ed.* **2016**, *55*, 4327−4331.
(14) Nakano, K.; Suemura, N.; Yoneda, K.; Kawata, S.; Kaizaki, S. Substituent Effect of the Coordinated Pyridine in a Series of Pyrazolato Bridged Dinuclear Diiron(II) Complexes on the Spin-Crossover Behavior. *Dalton Trans.* **2005**, 740−743.
(15) Park, J. G.; Jeon, I.-R.; Harris, T. D. Electronic Effects of Ligand Substitution on Spin Crossover in a Series of Diiminoquinonoid-Bridged $Fe(II)_2$ Complexes. *Inorg. Chem.* **2015**, *54*, 359−369.
(16) Jamula, L. L.; Brown, A. M.; Guo, D.; McCusker, J. K. Synthesis and Characterization of a High-Symmetry Ferrous Polypyridyl Complex: Approaching the $^5T_2/^3T_1$ Crossing Point for Fe(II). *Inorg. Chem.* **2014**, *53*, 15−17.
(17) Phan, H.; Hrudka, J. J.; Igimbayeva, D.; Lawson Daku, L. M.; Shatruk, M. A Simple Approach for Predicting the Spin State of Homoleptic Fe(II) Tris-Diimine Complexes. *J. Am. Chem. Soc.* **2017**, *139*, 6437−6447.
(18) Sharpe, A. G. *Inorganic Chemistry*, 3rd ed.; Longman Scientific & Technical: Essex, 1992.
(19) Cotton, F. A.; Wilkinson, G. *Advanced Inorganic Chemistry*, 5th ed.; Wiley: New York, 1988.
(20) Purcell, K. F.; Kotz, J. C. *An Introduction to Inorganic Chemistry*; Saunders College Publishing: Philadelphia, PA, 1980.
(21) Lindoy, L. F.; Livingstone, S. E. Complexes of Iron(II),Cobalt(II) and Nickel(II) with α-Diimines and Related Bidentate Ligands. *Coord. Chem. Rev.* **1967**, *2*, 173−193.
(22) Smith, A. P.; Fraser, C. L. In *Comprehensive Coordination Chemistry II*; Meyer, T. J., Ed.; Pergamon: Oxford, 2003; pp 1−23.
(23) Lever, A. B. P. Electrochemical Parametrization of Metal Complex Redox Potentials, Using the Ruthenium(III)/Ruthenium(II) Couple to Generate a Ligand Electrochemical Series. *Inorg. Chem.* **1990**, *29*, 1271−1285.
(24) Gorelsky, S. I.; Dodsworth, E. S.; Lever, A. B. P.; Vlcek, A. A. Trends in Metal−Ligand Orbital Mixing in Generic Series of Ruthenium N-Donor Ligand Complexes—Effect on Electronic Spectra and Redox Properties. *Coord. Chem. Rev.* **1998**, *174*, 469−494.
(25) Sarkar, B.; Suntrup, L. Illuminating Iron: Mesoionic Carbenes as Privileged Ligands in Photochemistry. *Angew. Chem., Int. Ed.* **2017**, *56*, 8938−8940.
(26) Becke, A. D. Density-Functional Exchange-Energy Approximation with Correct Asymptotic Behavior. *Phys. Rev. A: At., Mol., Opt. Phys.* **1988**, *38*, 3098−3100.
(27) Perdew, J. P. Density-Functional Approximation for the Correlation Energy of the Inhomogeneous Electron Gas. *Phys. Rev. B: Condens. Matter Mater. Phys.* **1986**, *33*, 8822−8824.
(28) Krishnan, R.; Binkley, J. S.; Seeger, R.; Pople, J. A. Self-Consistent Molecular Orbital Methods XX. A Basis Set for Correlated Wave Functions. *J. Chem. Phys.* **1980**, *72*, 650−654.
(29) McLean, A. D.; Chandler, G. S. Contracted Gaussian Basis Sets for Molecular Calculations. I. Second Row Atoms, Z = 11−18. *J. Chem. Phys.* **1980**, *72*, 5639−5648.
(30) Binning, R. C.; Curtiss, L. A. Compact Contracted Basis Sets for Third-Row Atoms: Ga−Kr. *J. Comput. Chem.* **1990**, *11*, 1206−1216.
(31) McGrath, M. P.; Radom, L. Extension of Gaussian-1 (G1) Theory to Bromine-Containing Molecules. *J. Chem. Phys.* **1991**, *94*, 511.
(32) Curtiss, L. A.; McGrath, M. P.; Blaudeau, J.-P.; Davis, N. E.; Binning, R. C.; Radom, L. Extension of Gaussian-2 Theory to Molecules Containing Third-Row Atoms Ga−Kr. *J. Chem. Phys.* **1995**, *103*, 6104.
(33) Dolg, M.; Wedig, U.; Stoll, H.; Preuss, H. Energy-Adjusted *ab initio* Pseudopotentials for the First Row Transition Elements. *J. Chem. Phys.* **1987**, *86*, 866−872.
(34) Bergner, A.; Dolg, M.; Küchle, W.; Stoll, H.; Preuß, H. *Ab initio* Energy-Adjusted Pseudopotentials for Elements of Groups 13−17. *Mol. Phys.* **1993**, *80*, 1431−1441.
(35) Frisch, M. J.; Trucks, G. W.; Schlegel, H. B.; Scuseria, G. E.; Robb, M. A.; Cheeseman, J. R.; Scalmani, G.; Barone, V.; Mennucci, B.; Petersson, G. A.; Nakatsuji, H.; Caricato, M.; Li, X.; Hratchian, H. P.; Izmaylov, A. F.; Bloino, J.; Zheng, G.; Sonnenberg, J. L.; Hada, M.; Ehara, M.; Toyota, K.; Fukuda, R.; Hasegawa, J.; Ishida, M.; Nakajima, T.; Honda, Y.; Kitao, O.; Nakai, H.; Vreven, T.; Montgomery, J. A., Jr.; Peralta, J. E.; Ogliaro, F.; Bearpark, M.; Heyd, J. J.; Brothers, E.; Kudin, K. N.; Staroverov, V. N.; Kobayashi, R.; Normand, J.; Raghavachari, K.; Rendell, A.; Burant, J. C.; Iyengar, S. S.; Tomasi, J.; Cossi, M.; Rega, N.; Millam, N. J.; Klene, M.; Knox, J. E.; Cross, J. B.; Bakken, V.; Adamo, C.; Jaramillo, J.; Gomperts, R.; Stratmann, R. E.; Yazyev, O.; Austin, A. J.; Cammi, R.; Pomelli, C.; Ochterski, J. W.; Martin, R. L.; Morokuma, K.; Zakrzewski, V. G.; Voth, G. A.; Salvador, P.; Dannenberg, J. J.; Dapprich, S.; Daniels, A. D.; Farkas, Ö.; Foresman, J. B.; Ortiz, J. V.; Cioslowski, J.; Fox, D. J. *Gaussian 09, revision D.01*; Gaussian, Inc.: Wallingford, CT, 2009.
(36) Gorelsky, S. I.; Lever, A. B. P. Electronic Structure and Spectra of Ruthenium Diimine Complexes by Density Functional Theory and Indo/S. Comparison of the Two Methods. *J. Organomet. Chem.* **2001**, *635*, 187−196.
(37) Gorelsky, S. I. *AOMix program*; http://www.sg-chem.net/.
(38) Glendening, E. D.; Badenhoop, J. K.; Reed, A. E.; Carpenter, J. E.; Bohmann, J. A.; Morales, C. M.; Landis, C. R.; Weinhold, F. *NBO 6.0*; Theoretical Chemistry Institute, University of Wisconsin: Madison, WI, 2013.

DOI: 10.1021/acs.inorgchem.8b01002
Inorg. Chem. 2018, 57, 9907−9917

(39) Reiss, H.; Heller, A. The Absolute Potential of the Standard Hydrogen Electrode: A New Estimate. *J. Phys. Chem.* **1985**, *89*, 4207−4213.
(40) Kelly, C. P.; Cramer, C. J.; Truhlar, D. G. Aqueous Solvation Free Energies of Ions and Ion−Water Clusters Based on an Accurate Value for the Absolute Aqueous Solvation Free Energy of the Proton. *J. Phys. Chem. B* **2006**, *110*, 16066−16081.
(41) Kelly, C. P.; Cramer, C. J.; Truhlar, D. G. Single-Ion Solvation Free Energies and the Normal Hydrogen Electrode Potential in Methanol, Acetonitrile, and Dimethyl Sulfoxide. *J. Phys. Chem. B* **2007**, *111*, 408−422.
(42) Fawcett, W. R. The Ionic Work Function and Its Role in Estimating Absolute Electrode Potentials. *Langmuir* **2008**, *24*, 9868−9875.
(43) Tissandier, M. D.; Cowen, K. A.; Feng, W. Y.; Gundlach, E.; Cohen, M. H.; Earhart, A. D.; Coe, J. V.; Tuttle, T. R. The Proton's Absolute Aqueous Enthalpy and Gibbs Free Energy of Solvation from Cluster-Ion Solvation Data. *J. Phys. Chem. A* **1998**, *102*, 7787−7794.
(44) Tissandier, M. D.; Cowen, K. A.; Feng, W. Y.; Gundlach, E.; Cohen, M. H.; Earhart, A. D.; Tuttle, T. R.; Coe, J. V. The Proton's Absolute Aqueous Enthalpy and Gibbs Free Energy of Solvation from Cluster Ion Solvation Data. *J. Phys. Chem. A* **1998**, *102*, 9308−9308.
(45) Zhan, C.-G.; Dixon, D. A. Absolute Hydration Free Energy of the Proton from First-Principles Electronic Structure Calculations. *J. Phys. Chem. A* **2001**, *105*, 11534−11540.
(46) Baik, M.-H.; Friesner, R. A. Computing Redox Potentials in Solution: Density Functional Theory as a Tool for Rational Design of Redox Agents. *J. Phys. Chem. A* **2002**, *106*, 7407−7412.
(47) Paulsen, H.; Duelund, L.; Winkler, H.; Toftlund, H.; Trautwein, H. X. Free Energy of Spin-Crossover Complexes Calculated with Density Functional Methods. *Inorg. Chem.* **2001**, *40*, 2201−2203.
(48) Ghosh, A.; Taylor, P. R. High-Level *ab initio* Calculations on the Energetics of Low-Lying Spin States of Biologically Relevant Transition Metal Complexes: A First Progress Report. *Curr. Opin. Chem. Biol.* **2003**, *7*, 113−124.
(49) Ghosh, A. Transition Metal Spin State Energetics and Noninnocent Systems: Challenges for DFT in the Bioinorganic Arena. *JBIC, J. Biol. Inorg. Chem.* **2006**, *11*, 712−724.
(50) Conradie, J.; Ghosh, A. DFT Calculations on the Spin-Crossover Complex Fe(Salen)(NO): A Quest for the Best Functional. *J. Phys. Chem. B* **2007**, *111*, 12621−12624.
(51) De Angelis, F.; Jin, N.; Car, R.; Groves, J. T. Electronic Structure and Reactivity of Isomeric Oxo-Mn(V) Porphyrins: Effects of Spin-State Crossing and pK_a Modulation. *Inorg. Chem.* **2006**, *45*, 4268−4276.
(52) Ghosh, A.; Vangberg, T.; Gonzalez, E.; Taylor, P. Molecular Structures and Electron Distributions of Higher-Valent Iron and Manganese Porphyrins. Density Functional Theory Calculations and Some Preliminary Open-Shell Coupled-Cluster Results. *J. Porphyrins Phthalocyanines* **2001**, *05*, 345−356.
(53) Bowman, D. N.; Jakubikova, E. Low-Spin Versus High-Spin Ground State in Pseudo-Octahedral Iron Complexes. *Inorg. Chem.* **2012**, *51*, 6011−6019.
(54) This is expected because it is a pure GGA functional. In addition, the quintet−singlet energy gap for the unsubstituted complex is known and we can confirm that BP86 does overstabilize the singlet.
(55) Hansch, C.; Leo, A. *Substituent Constants for Correlation Analysis in Chemistry and Biology*; Wiley: New York, 1979.
(56) Hansch, C.; Leo, A.; Taft, R. W. A Survey of Hammett Substituent Constants and Resonance and Field Parameters. *Chem. Rev.* **1991**, *91*, 165−195.
(57) Zakeeruddin, S. M.; Fraser, D. M.; Nazeeruddin, M. K.; Grätzel, M. Towards Mediator Design: Characterization of Tris-(4,4′-Substituted-2,2′-Bipyridine) Complexes of Iron(II), Ruthenium(II) and Osmium(II) as Mediators for Glucose Oxidase of *Aspergillus niger* and Other Redox Proteins. *J. Electroanal. Chem.* **1992**, *337*, 253−283.
(58) $[Fe(bpy)_3]^{2+}$ belongs to the D_3 point group, and so it is inappropriate to label any orbital as t_{2g}. As the complex is pseudo-octahedral, however, there are several orbitals that resemble the t_{2g} orbitals expected for a perfectly octahedral molecule (O_h). For readability's sake these orbitals will be referred to as t_{2g} throughout.
(59) Gorelsky, S. I.; Ghosh, S.; Solomon, E. I. Mechanism of N_2O Reduction by the μ_4-S Tetranuclear Cu_z Cluster of Nitrous Oxide Reductase. *J. Am. Chem. Soc.* **2006**, *128*, 278−290.
(60) Daul, C.; Baerends, E. J.; Vernooijs, P. A Density Functional Study of the MLCT States of $[Ru(bpy)_3]^{2+}$ in D_3 Symmetry. *Inorg. Chem.* **1994**, *33*, 3538−3543.
(61) Kitaura, K.; Morokuma, K. A New Energy Decomposition Scheme for Molecular Interactions within the Hartree-Fock Approximation. *Int. J. Quantum Chem.* **1976**, *10*, 325−340.
(62) Ziegler, T.; Rauk, A. On the Calculation of Bonding Energies by the Hartree Fock Slater Method. *Theor. Chim. Acta* **1977**, *46*, 1−10.
(63) Note that in this study when $\Delta\Delta E_{prep}$ was considered, it only entailed comparing the energies of the $(bpy^Y)_3$ fragments themselves, and hence no actual optimizations of the isolated bpy^Y ligands needed to be performed.
(64) Using AOMix with Gaussian, it was not possible to resolve the steric interactions into their electrostatic and repulsive components, and therefore only the steric interactions are considered in this study.
(65) Lord, R. L.; Baik, M.-H. Why Does Cyanide Pretend to Be a Weak Field Ligand in $[Cr(CN)_5]^{3-}$? *Inorg. Chem.* **2008**, *47*, 4413−4420.

DOI: 10.1021/acs.inorgchem.8b01002
Inorg. Chem. 2018, 57, 9907−9917